Eur. Phys. J. B **60**, 493–498 (2007)
DOI: 10.1140/epjb/e2008-00010-8

THE EUROPEAN PHYSICAL JOURNAL B

Scaling and self-similarity in $Pb_{1-x}Fe_xS$ nanoparticle films

V. Banerjee[a]

Department of Physics, Indian Institute of Technology, Hauz Khas, New Delhi 110016, India

Received 18 June 2007 / Received in final form 15 November 2007
Published online 16 January 2008 –

Abstract. This paper addresses the issues of scaling and self-similarity in typical nanoparticle films. The role played by microscopic processes contributing to growth on these issues is probed. While we perform this investigation for a specific system viz., $Pb_{1-x}Fe_xS$ nanoparticle films for clarity of the procedures, the analysis is general and can be applied to a variety of systems obtained using different deposition techniques.

PACS. 61.43.Hv Fractals; macroscopic aggregates – 68.55.A Nucleation and growth: microscopic aspects – 68.55.J Structure and morphology; thickness; crystalline orientation and texture

1 Introduction

The formation of nanostructures is a complex process involving competition between nucleation and growth of particles. These processes occur with characteristic rates governed by experimental conditions. They affect the morphology of the evolving structures to varying degrees. A simple picture of a typical growth process can be visualized on a two dimensional substrate as follows. Monomers are dropped with a specified flux rate at random positions on the substrate. Each monomer, as revealed by atomic scale measurements, is either adsorbed by the substrate or undergoes a random walk on the substrate until one of the following occurs [1,2]. It finds an existing particle (of two or more monomers) and gets incorporated leading to growth or finds diffusing monomers and nucleates to yield a new particle. Not only small particles, but large particles comprising of a several hundred monomers are also found to be mobile, but with a lower mobility. Further, the possibility of loss of mass due to desorption of a monomer or chipping of a bit of mass from a particle have also been observed. As a result these structures are continuously evolving and highly non-equilibrium in nature.

The random deposition of monomers and the Brownian trajectories traced by particles due to surface diffusion introduces a strong element of stochasticity in the above system. Growing surfaces governed by stochastic processes are often known to yield structures having no characteristic length or time scale [3,4]. One procedure for this identification is provided by concepts from scaling theories [5,6]. It is a feature of objects or laws that do not change if length-scales (or energy scales) undergo a dilation. Mathematically, scale invariance refers to an invariance of individual functions or curves under a discrete set of dilations. The requirement for a function $f(x)$ to be invariant under some scale factor α is $f(x) = \alpha^{-\beta} f(\alpha x)$ where β is the scaling exponent. If different data sets can be made to collapse on a universal curve with the help of the proposed dilation or scaling function $f(x)$, they are said to exhibit scaling. The data sets then rely on the same mechanisms for their formation and the evolving system is said to be scale-invariant.

A closely related issue to scaling is that of self-similarity. The later implies an invariance under an isotropic transformation such as a simple dilation. If we consider an object comprising of a set of points $R = (x_1, x_2,....)$, a dilation with a scaling factor α changes the coordinates to $\alpha R = (\alpha x_1, \alpha x_2,....)$. The set so formed is self-similar if it is invariant under this transformation. Self-similarity is strictly found in deterministic fractals such as the Koch curve or the Serpienski gasket in which, the rescaled system is identical to the original system. Natural structures such as growing interfaces on the other hand exhibit statistical self-similarity within a certain regime of the parameter space due to the inherent randomness in their contributory process. Thus only statistical quantities are the same for the rescaled and the original system.

Another procedure for investigating self-similarity in a system is obtained by computing quantities which are typically used to characterize fractals. The most commonly computed quantity is the fractal dimension [7,8]. A non-integer value implies fractality and hence self-similarity. There are many definitions of fractal dimension such as the box counting or the Haussdorf dimension, the information dimension and the correlation dimension to name a few. We find that the later, usually calculated in the context of strange attractors, is especially useful to identify self-similarity in growing structures. Further, the value of

[a] e-mail: varsha@physics.iitd.ernet.in

the fractal dimension is known to have a significant influence on the dynamics of growth process.

In an earlier publication we proposed the underlying microscopic growth mechanisms contributing to the formation of $Pb_{1-x}Fe_xS$ nanoparticle films [9]. We also found that the particle-size distributions corresponding to different flux rates exhibited scaling hinting towards the presence of self-similarity in the growth process. A more relevant quantity for the identification of scale-invariance though, is the inter-particle separation r. Hence, in this paper, we concentrate on the calculation and analysis of the probability distributions $P(r)$, which give the conditional probability of finding a particle of any size separated by a distance r from a specified one, corresponding to varying flux rates. The main results of this study are summarized below. The distributions $P(r)$ are bimodal for all the values of flux considered indicating the presence of two dominant growth mechanisms in the system. The cumulative probability distributions constructed from the above separation distributions exhibit scaling. We then check for self-similarity using transmission electron microscopy (TEM) images of the $Pb_{1-x}Fe_xS$ depositions. The cumulative probability distributions readily provide the correlation dimension of the nanoparticle films. Its non-integer value of 1.72 ± 0.01 reiterates self-similarity. We identify the experimental conditions under which scaling and self-similarity are expected to arise. Arguments have been developed to explain the experimental observations in terms of a diffusion-aggregation model introduced earlier in [9]. Thus the present study is an effort to obtain further insight on the growth of $Pb_{1-x}Fe_xS$ nanoparticle films to supplement the results of [9].

The paper is organized as follows. The experimental procedure for obtaining $Pb_{1-x}Fe_xS$ nanoparticle films is briefly described in Section 2. The scaling analysis is performed in Section 3. Aspects of self-similarity and evaluation of the correlation dimension are attended to in Section 4. A short conclusion is provided in Section 5.

2 Experimental procedure

The procedure for obtaining $Pb_{1-x}Fe_xS$ nanoparticle films is outlined in detail in [9]. However the key steps are reproduced below for the sake of completeness. A chemical bath deposition (CBD) method was used to obtain ternary $Pb_{1-x}Fe_xS$ nanoparticle films on a silicon substrate. A typical medium in the CBD process consists of one or more metal salts, a source for the chalcogenide X (= S, Te, Se) and a chelating agent to limit the hydrolysis of the metal ion and impart stability to the bath which would otherwise undergo rapid hydrolysis and precipitation. More specifically, aqueous solutions of $(M/25)$ lead acetate, $(M/25)$ ferrous chloride and $(M/20)$ thiourea, all maintained at 30 °C and stirred continuously, were used to obtain $Pb_{0.5}Fe_{0.5}S$ semiconductor films. Optimized quantities of precursors to achieve a specific composition of x were obtained by analyzing x-ray fluorescence data from test films grown under identical conditions. The chemical reaction which results in the production of $Pb_{1-x}Fe_xS$ "monomers" is described below:

$$(1-x)\mathrm{Pb(CH_3COO)_2} + x\mathrm{FeCl_2} + \mathrm{(NH_2)_2CS} \xrightarrow{\mathrm{NH_4OH}} \mathrm{Pb_{1-x}Fe_xS} + \mathrm{CH_3COOH} + \mathrm{NH_4Cl}.$$

One important parameter expected to affect the growth process is the rate of formation of $Pb_{1-x}Fe_xS$ monomers or the incident flux on the substrate. In the above experiment, this was controlled by the availability of S^{2-} ions produced by the hydrolysis of thiourea in the basic medium. An increase in their concentration was achieved by increasing the pH of the chemical bath by the addition of liquor ammonia. The later provides excess (OH^-) ions which consequently increases the concentration of S^{2-} ions and hence $Pb_{1-x}Fe_xS$ monomers. Films with three different pH values of the chemical bath, viz., 9.25, 10.0 and 10.75 were grown for optimized times to obtain a thickness of approximately 30 nanometers. A TEM of the deposited films was carried out in a plane-view mode using a Philips CM20 instrument to study features related to the growth process. These micrographs are shown in Figures 1a–1c in [9]. We refer the reader to these to avoid replication.

3 Scaling analysis

We now proceed to obtain probability distributions of the inter-particle separations in the deposited films. This information is obtained from the above TEM micrographs by the following procedure. As we are interested in aspects related to scaling, we do away with scaling-irrelevant features such as details of particle shapes by suppressing the structure of the particles and resorting to a "point particle" representation. These are shown in Figures 1a–1c for the corresponding TEM micrographs of [9] for three values of $pH = 9.25$, 10.0 and 10.75 that were considered. Such a representation preserves information regarding density, placement and regions devoid of particles. We also mention here that the point particle model has been the starting point of several theoretical descriptions of epitaxial growth, the most widely used and analyzed being the Smoluchowski rate equation approach [10]. The inter-particle separation r was determined from scanned images of the above point representations by writing a simple computer program. Each point was considered and its distance of separation from every other point in the point particle representation was computed. Thus if the number of points in the representation is N, a total of $N(N-1)$ separations were obtained. These were then binned appropriately to find the probability $P(r)$ for a pair to have an inter-particle separation of r.

The above procedure was carried out for all the three point particle representations in Figures 1a–1c for the three pH values. The corresponding probability distributions are shown in Figure 2. The distributions are bimodal in nature. Multimodal distributions have been observed in

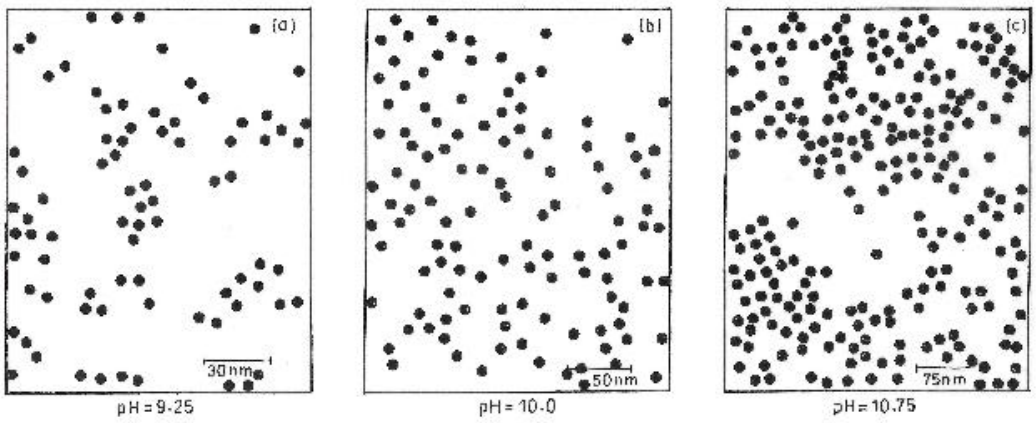

Fig. 1. Point representations of the TEM images of $Pb_{0.5}Fe_{0.5}S$ nanoparticle films for three different values of pH equal to (a) 9.25, (b) 10.0 and (c) 10.75.

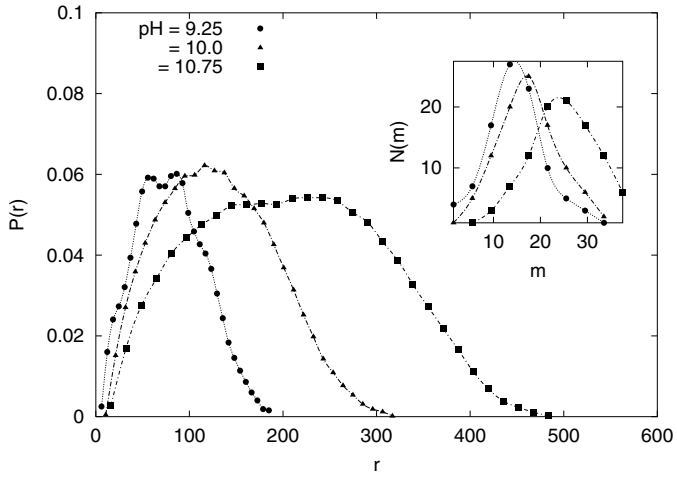

Fig. 2. (a) Probability distribution of inter-particle separation in $Pb_{0.5}Fe_{0.5}S$ nanoparticle films for the three different values of pH of the chemical bath. The inset shows the distribution of particle sizes in the nanoparticle films for the corresponding values of pH.

many growth processes, especially in the context of colloids, and have been attributed to the presence of variable growth mechanisms [11]. In the present context, the bimodal distribution is expected to result from two dominant particle growth mechanisms which we shall identify shortly. We wish to point out here that the broadening of probability distributions and the increase in the average inter-particle separation with pH is not an effect of the later, but has more to do with the larger scale of the TEM images corresponding to samples with higher values of pH. The respective scales are indicated in Figures 1a–1c. We have checked that these distributions collapse onto a master curve when viewed on the same lengthscale. This invariance amongst distributions corresponding to different pH values is a consequence of self-similarity in the growth process and is addressed in Section 4.

In our earlier studies, we found the following model suitable to describe the experimentally observed features of nanoparticle growth in $Pb_{1-x}Fe_xS$ and Pd depositions [9,12]. The two primary mechanisms which we assumed were (i) irreversible adsorption of monomers with a rate F on the substrate and (ii) their subsequent diffusion and aggregation upon collision to form larger particles. In order to mimic the experimentally observed asymmetrical and peaked particle size distributions $N(m)$, we found that it is essential to assume a power law dependence of diffusivity D_m on the mass m of the particle, i.e., $D_m \sim m^{-\mu}$. A mass-independent diffusibility corresponding to a value of $\mu = 0$ resulted in a steady state size distribution as a time independent power law $N(m) \sim m^{-\tau}$ with the exponent $\tau = 1.45 \pm 0.01$. On the other hand, a value of $\mu > 1$ implying higher mobility for smaller particles as compared to larger particles, reproduced many of the qualitative features of the experimentally observed particle size distributions. These observations were made in both the Monte Carlo simulations as well as the mean field analysis of the Smoluchowski rate equations of the described model. The other microscopic mechanisms which could affect growth were desorption of a monomer or fragmentation of a bit of mass from the particle. However scanning tunneling microscopy measurements at near room temperature have revealed that the rate of escape of monomers or bits of mass is negligible compared to the rate of surface diffusion making aggregation an irreversible process [13,14]. Thus by elimination, the observed bimodal distribution of Figure 2 can be attributed to the mechanisms of adsorption and irreversible aggregation which dominate at room temperature.

Typical aggregation mechanisms observed in the context of coalescence phenomena are those of Ostwald ripening and/or cluster migration [15]. In Ostwald ripening, the larger particles grow or "ripen" at the expense of the smaller ones due to their desire to minimize the surface free energy. In cluster migration on the other hand, coalescence occurs as a result of collision of particles as they execute a random walk on the substrate. It is difficult to distinguish Ostwald ripening from cluster mobility coalescence in experiments. However, their presence is characterized by (a) an increased mean volume of particles,

(b) a decreased density or coverage of the substrate and (c) a broadening of the particle size distribution. Each of these features are indeed observed in Figure 2, strengthening our belief of adsorption and mass-dependent diffusion being the two major contributors towards growth of $Pb_{1-x}Fe_xS$ nanoparticles. The inset of Figure 2 depicts the effect of increasing pH on $N(m)$, the number of particles of size m. This information was obtained in our earlier study from the same set of TEM images which have been used to obtain the point particle representations of Figures 1a–1c [9]. The main effect of increasing the pH of the chemical bath, as observed from the inset of Figure 2, is to broaden the distributions and increase the average size m_{av}. Recalling that its role is to provide S^{-2} ions for the formation of $Pb_{1-x}Fe_xS$ monomers on the substrate, the pH may be identified with an adsorption rate in a deposition experiment. Naively, one expects the average inter-particle separation to decrease with increasing adsorption rate due to an enhanced particle density on the substrate. However, the data of Figure 2 suggests that the additional monomer adsorption is counterbalanced by microscopic growth moves which create large, well separated particles.

We now address the main issue of this paper, namely that of scaling in the nanoparticle films obtained under different growth conditions. To do this, we construct $C(r)$ which is the conditional probability of finding a particle of any size at a distance less than or equal to r. The reasons for using $C(r)$ rather than $P(r)$ to probe scaling is because the former has been found to be more suitable to obtain information about (i) depletion of concentration of pairs of particles with small separation as compared to r_{av}, (ii) the cross-over behavior to large separation and (iii) to demonstrate scaling with respect to r_{av} [14,18]. We postulate the following scaling ansatz for the cumulative separation distributions corresponding to different values of pH:

$$C(r) = \frac{1}{r_{av}} f\left(\frac{r}{r_{av}}\right). \qquad (1)$$

It satisfies the requirements of normalization and $f(0)$ is 0 while f(x$\rightarrow \infty$) $\rightarrow$ 1. Equation (1) implies that a plot of $r_{av}C(r)$ as a function of r/r_{av} should bring about a collapse of the distributions corresponding to different pH values onto a universal curve in case the data exhibit scaling. This is indeed true, as seen in Figure 3, implying that the only relevant variable for determining the above distributions is r_{av}. The corresponding unscaled data are shown in the inset.

Some comments regarding the scaling ansatz of equation (1) are in order. A rate equation analysis for the proposed theoretical description of the growth phenomena in I was carried out by Krapivsky et al. within a mean field approximation [16,17]. Steady state particle-size distributions were obtained which exhibited scaling with respect to the incident flux. The features related to spatial distribution however are hard to incorporate in a rate equation treatment making it difficult to predict a scaling function for the distributions $P(r)$ or $C(r)$ [18]. The usual course then is to postulate a scaling form for the separation distribution on the basis of heuristic arguments. Another form given by $C(r) = N^{-1} f(r/r_{av})$ proposed in [18] was found to be useful in scaling of separation distributions of Iron islands in the initial stages of growth [14]. Here N represented the total number of particles excluding monomers and the scaling ansatz was used to collapse data corresponding to different temperatures. This was observed in the context of Iron-on-Iron depositions at different temperatures [14]

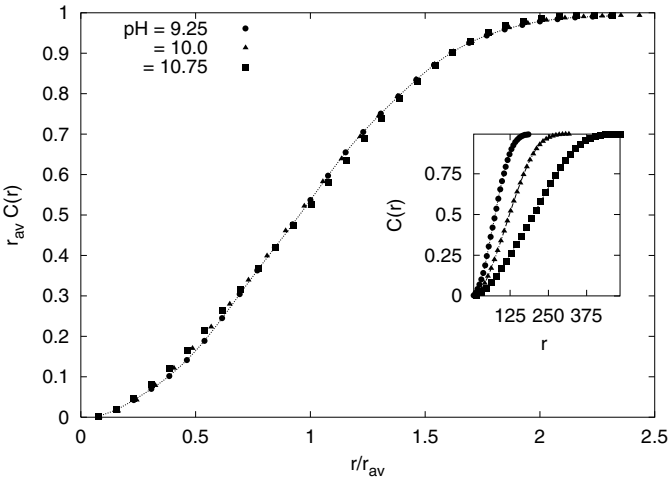

Fig. 3. Scaled cumulative separation distribution described by equation (1) for the three values of pH considered. The inset shows the corresponding unscaled data.

4 Self-similarity and the fractal dimension

The self-similarity in the deposited films corresponding to different pH values can be easily checked by appropriate dilations of Figures 1b and 1c corresponding to pH = 10.0 and 10.75 respectively in order to view them on the same length scale as that of Figure 1a which corresponds to a pH value of 9.25. Thus the required dilation for Figures 1b and 1c are 1.6 and 2.5 respectively. The dilated images are shown in Figures 4a and 4c. With this, the scales of Figures 1a, 4a and 4c corresponding to pH = 9.25, 10.0 and 10.75 respectively are identical. The statistical self-similarity in these sets of figures is notable. Similarly, a magnification by a factor of 1.5 of Figure 1c corresponding to pH = 10.75 yields an image bearing the same scale as Figure 1b which corresponds to pH = 10.0. The magnified image is shown in Figure 4b. Here again, we can observe the statistical self-similarity between the two images. At this juncture, we remind the reader of the comments related to Figure 2 regarding the invariance of inter-particle separation distributions with pH. The statistical self-similarity in the images discussed above makes this invariance evident.

An alternative procedure could be to determine the correlation dimension d_c of an attractor responding to the growth process [21]. To do so, we first need to define the correlation sum $C(\tilde{r})$. Traditionally, it is obtained

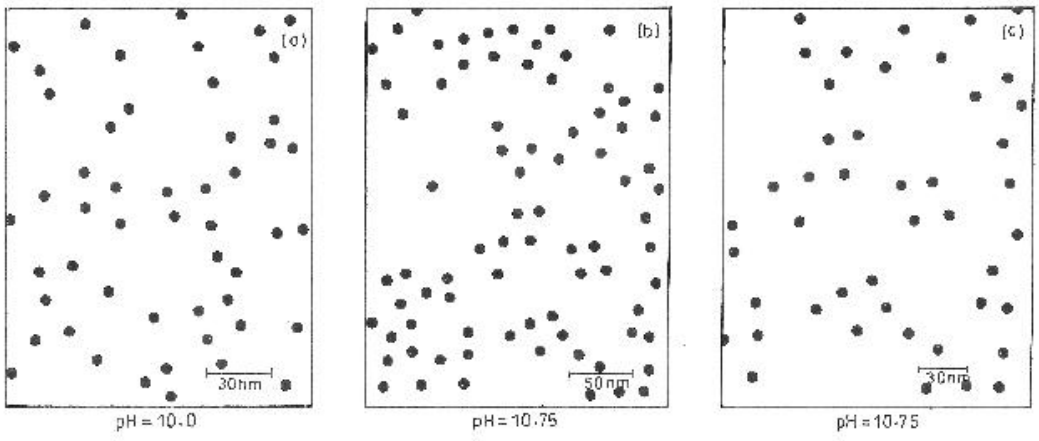

Fig. 4. Dilated portions (lower right corner) of Figures 1b and 1c. The scales in the images are to be noted and appropriate pH values are to be compared with those in Figure 1 (refer text in Sect. 4).

by considering correlations between points of a long time-series. denoting the N points of such a time series by $\vec{X}_i = \vec{X}(t + i\tau)$, where τ is an arbitrary but fixed increment. The definition of the correlation sum is:

$$C\tilde{(}r) = \frac{1}{N^2} \sum_{i,j=1}^{N} \Theta \left(r - \mid \vec{X}_i - \vec{X}_j \mid \right), \qquad (2)$$

where Θ is a Heaviside function, r is the radius of an n-dimensional hyper sphere centered on each point. The Heaviside function is equal to unity (zero) if the value inside the brackets is positive (negative). X_i is the reference point and X_j are the other points in the time series. Thus the Heaviside function counts all points within the hyper sphere of radius r. The cumulative sum of all counted points is then divided by the total number of pairs N^2 to give $C\tilde{(}r)$. The maximum value of $C\tilde{(}r)$ is unity, when r is greater than the largest distance between two points on the attractor and hence all pairs are counted. The minimum value of $C\tilde{(}r)$ is $2/N^2$ when only the two closest points are counted. In case of self-similar structures, $C\tilde{(}r)$ behaves as a power law of r with a non-integer power which is the correlation dimension d_c:

$$C\tilde{(}r) \propto r^{d_c} \qquad (3)$$

d_c is closely related to the Haussdorf dimension and can be taken as a most useful measure of the local structure of the attractor [21]. It can be obtained in a straight-forward fashion from the data in the inset of Figure 3. We show these data on a double logarithmic scale in Figure 5. The value of d_c from the slope of the best fit line to the central portion of the data is found to be 1.72 ± 0.01. This evaluation is yet another test for the presence of self-similarity in the non-equilibrium growing structure for the low flux rates considered during deposition.

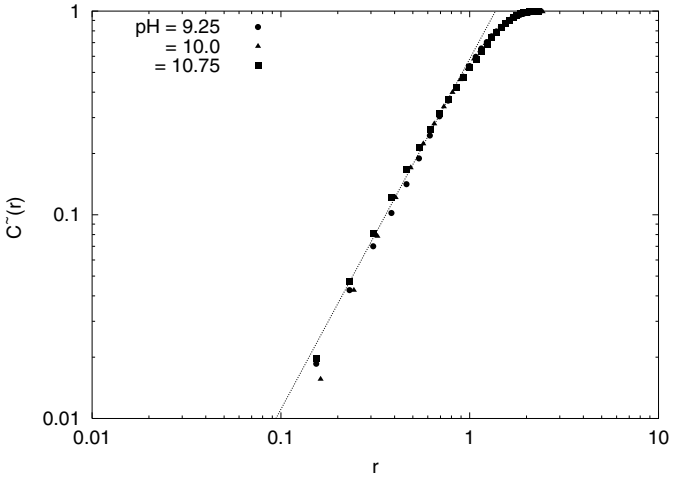

Fig. 5. The correlation sum defined by equation (2) on a double logarithmic scale. The correlation dimension $d_c = 1.72 \pm 0.01$ is given by the slope of the best-fit (dashed) line.

5 Conclusion

In conclusion, we have probed the presence of scaling and self-similarity in the non-equilibrium growth process of $Pb_{1-x}Fe_xS$ nanoparticle films obtained at room temperature for different values of the incident monomer flux. The distributions corresponding to inter-particle separations are observed to be bimodal. We attribute this form to the presence of two dominant mechanisms contributing to growth viz., adsorption of monomers and their subsequent diffusion and aggregation. The main effect of increasing monomer flux is to increase the average inter-particle separation and broaden the distributions. This is understood by proposing the aggregation mechanism to be a akin to Ostwald ripening and cluster migration typically discussed in the context of coalescence phenomena. The cumulative probability distributions were seen to exhibit scaling, indicating the absence of characteristic length scales as well as time scales for the experimental conditions of low flux

rates and short deposition times. We also addressed the issue of self-similarity. Due to the stochastic nature of both, the adsorption and the diffusion process, the growth process leading to the formation of nanoparticle films is self-similar. We checked this by two procedures. The first one used concepts of scaling while the second one involved the calculation of fractal dimension. We conclude from these analyses that the growth process is self-similar for low flux rates and short deposition times thereby allowing the particles to diffuse on the substrate in the form of a Brownian walk. The substrate temperature is expected to play an important role on this issue as it features in the diffusion rates of particles [4]. For instance at very low temperatures monomer adsorption will be the only mechanism of growth. Finally although we have studied a specific system viz., $Pb_{1-x}Fe_xS$ nanoparticle films for clarity of procedures, the analyses are generic and can be applied to a variety of systems obtained using different deposition techniques.

I thank R. Ramaswamy for useful inputs in the evaluation of the correlation dimension. I am also thankful to L.K. Malhotra for critical comments on the manuscript.

References

1. *Kinetics of Ordering and Growth at Surfaces*, Vol. 239 of NATO Advanced Study Institute, Series B: Physics, edited by M. Lagally (Plenum, New York, 1990)
2. *Morphological Organization of Epitaxial Growth and Removal*, edited by Z. Zang, M.G. Lagally (World Scientific, Singapore, 1998)
3. T. Vicsek, *Fractal Growth Phenomena* (World Scientific, Singapore, 1992)
4. A.-L. Barabasi, H.E. Stanley, *Fractal Concepts in Surface Growth* (Cambridge University Press, 1995)
5. J. Feder, *Fractals*, Chapter 2 (Plenum Press, New York, 1988)
6. *Dynamics of Fractal surfaces*, edited by F. Family, T. Vicsek (World Scientific, Singapore, 1991)
7. P.S. Addison, *Fractals and Chaos* (Overseas Press, 2005)
8. J.L. McCauley, *Chaos, Dynamics and Fractals* (Cambridge University Press, 1993)
9. V. Banerjee, R.K. Joshi, H.K. Sehgal, Phys. Rev. E **70**, 036122 (2004)
10. M.V. Smoluchowski, Phys. Z **17**, 557 (1916); Z. Phys. Chem. **92**, 129 (1917)
11. S.K. Friedlander, *Smoke, Dust and Haze: Fundamentals of Aerosol Behavior* (Wiley, Ney York, 1977)
12. V. Agarwal, I. Aruna, V. Banerjee, B.R. Mehta, Phys. Rev. B **74**, 035412 (2006)
13. Y.-W. Mo, J. Kleiner, M.B. Webb, M.G. Lagally, Phys. Rev. Lett. **66**, 1998 (1991)
14. J.A. Stroscio, D.T. Pierce, Phys. Rev. B **49** R8522 (1994)
15. Milton Ohring, *The Materials Science of Thin Films* (Academic Press, USA, 2002)
16. P.L. Krapivsky, S. Redner, Phys. Rev. E **54**, 3553 (1996)
17. P.L. Krapivsky, J.F.F. Mendes, S. Redner, Phys. Rev. B **59**, 15950 (1999)
18. M.C. Bartlet, J.W. Evans, Phys. Rev. B **46**, 12675 (1992)
19. M.C. Bartlet, M.C. Tringides, J.W. Evans, Phys. Rev. B **47**, 13891 (1993)
20. L. Kuipers, R.E. Palmer, Phys. Rev. B **53**, R7646 (1996)
21. P. Grassberger, I. Procaccia, Phy. Rev. Lett. **50**, 346 (1983); P. Grassberger, I. Procaccia, Physica D **9**, 189 (1983)